Inorganic Chemistry

Article

pubs.acs.org/IC

Structural and Electric Evidence of Ferrielectric State in Pb_2MnWO_6 Double Perovskite System

Fabio Orlandi,*[,†] Lara Righi,[†,§] Riccardo Cabassi,[§] Davide Delmonte,[‡,§] Chiara Pernechele,[‡] Fulvio Bolzoni,[§] Francesco Mezzadri,[†] Massimo Solzi,[‡] Marco Merlini,[∥] and Gianluca Calestani[†,§]

[†]Dipartimento di Chimica, Università di Parma, Parco Area delle Scienze 17/A, 43124 Parma, Italy

[‡]Dipartimento di Fisica e Scienze della Terra, Università di Parma, Parco Area delle Scienze 7/A, 43124 Parma, Italy

[§]IMEM-CNR, Parco Area delle Scienze 37/A, 43124 Parma, Italy

[∥]Dipartimento di Scienze della Terra, Università di Milano, Via Mangiagalli 34, 20133 Milano, Italy

Supporting Information

ABSTRACT: In this paper we describe the new ferri-electric compound Pb_2MnWO_6 (PMW), a double perovskite that can be considered as a novel structural prototype showing complex nuclear structure and interesting electric properties. According to single-crystal synchrotron data, PMW crystallizes in the noncentrosymmetric polar group $Pmc2_1$, in which the two symmetry-independent lead atoms give rise to a ferrielectric arrangement. The accurate crystallographic characterization indicates the presence of a complex distortion of the perovskite lattice driven by the local instability induced by the $6s^2$ lone pair of the lead atoms. These peculiar structural features are confirmed by the complete electrical characterization of the system. Dielectric and transport measurements indicate an insulating character of the sample, while pyroelectric measurements point out a ferrielectric state characterized by different contributions. The magnetic transition at 45 K is accompanied by a magnetostrictive effect indicating a probable spin−lattice coupling. The characterizations carried out on PMW, showing the evidence of a coexistence of antiferromagnetism and ferrielectricity at low temperature, could lead to the definition of a new class of multiferroic materials.

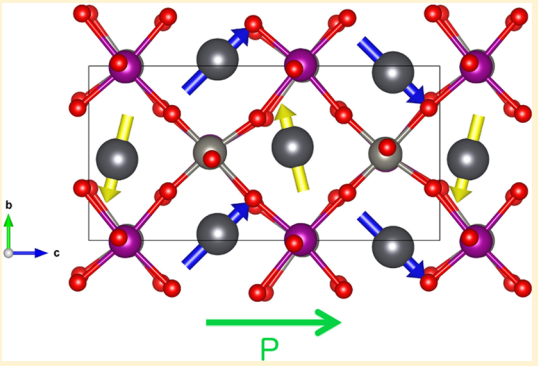

INTRODUCTION

Multiferroic materials have recently attracted great interest in materials science inspiring the design of new multifunctional applications. Besides the possible applications, the combination of magnetism and ferroelectricity in single-phase materials represents a great challenge also in fundamental science, where it is still an open issue regarding the understanding of the coexistence of the ferroic orders, which in principle mutually exclude each other.[1] In this scenario, compounds with perovskite structure represent a promising playground, because of the particular ability of this structure to arrange atomic species with different ionic radii and functionalities via lattice distortion. Interestingly double perovskites with formula $A_2BB'O_6$ are featured by the ordered distribution at the B site of two different cations showing specific dimensions and charge, typically assuming the rock salt type of ionic packing. Previous investigations showed that the presence of two different transition metals within the perovskite framework might determine remarkable magnetic and electric properties, such as low-field magnetoresistance, ferrimagnetism, and multiferroicity.[2−5]

In recent years, lead-based double perovskites have received much attention in reference to their notable dielectric and piezoelectric properties,[4−9] arising from the local distortion given by the $6s^2$ lone pair character of the Pb^{2+} ion. On the other hand, in analogy with bismuth-based multiferroics,[10] magnetic ordering may be achieved in these compounds by introducing proper magnetic ions in the B and B′ sites, finally allowing to fine-tune the exchange interactions and drive the physical properties of the systems. However, because of their "dual" character, the observed structural and physical properties are very sensitive to the presence of cationic order at the B site; for instance, partial or complete disorder can produce diffuse phase transitions and properties like relaxor ferroelectricity.[11]

Lately Blasco et al.[9] reported that the Pb_2MnWO_6 (PMW) perovskite is characterized at room temperature (RT) by a crystal structure with orthorhombic symmetry associated with high values of the dielectric constant. The authors described the system by using the centrosymmetric *Pnma* space group, emphasizing the presence of an antipolar electric state called antiferroelectric phase. The published work is mainly focused on the structural and electrical behavior of PMW at high temperature. It was found that the system undergoes, by approaching 445 K, an antiferro to paraelectric transition related to the setting of cubic symmetry.[12] In addition, a

Received: June 6, 2014
Published: September 8, 2014

magnetic transition close to T_a = 45 K was observed and ascribed to antiferromagnetic ordering.[9] Within this framework PMW can be reasonably considered as a multiferroic material having the co-occurrence of electric and magnetic ordering below 45 K. It is worth underlining that the antiferroelectric polar state is considered particularly unusual for mixed oxides owing to the structural and electrical conditions necessary to allow this type of electric ordering. As a consequence only few works are known wherein the antiferroelectric state is completely characterized from both the electric and structural point of view. Furthermore, the multiferroism associated with the conjugation of antipolar electric and magnetic ordering represents an outstanding case deserving to gather more attention. The simultaneous presence of antiferroelectricity and antiferromagnetism is largely unexplored by the actual scientific production and the extended investigation of such intriguing class of materials could provide unexpected insights.

In this work the exhaustive structural analysis of the PMW crystal structure associated with the antiferroelectric state is presented. The structural analysis carried out by using single-crystal data evidenced the presence of a noncentrosymmetric structure excluding the existence of a clear antiferroelectric polar condition. Furthermore, to get valuable information regarding the supposed multiferroic state, the low-temperature behavior was investigated by electric and structural characterizations.

EXPERIMENTAL SECTION

The PMW sample was synthesized by solid-state reaction. Stoichiometric amounts of PbO, $MnCO_3$, and WO_3 were ground and fired at 800 °C for 2 h in N_2 stream. The obtained powder was regrounded, pressed into pellets, and sintered at 820 °C for 4 h. The phase purity was checked by powder X-ray diffraction (PXRD) using a Thermo ARL X'tra diffractometer equipped with Cu Kα radiation and a Si(Li) Thermo Electron solid-state detector to eliminate the fluorescence of manganese. Temperature-dependent patterns were collected on the same diffractometer by using an Anton Paar TTK450 chamber in the temperature range of 90−500 K.

Single-crystal data were collected at RT from a crystal isolated from the powder sample with dimensions 2 × 2 × 2 μm^3 at the D09A beamline of the European Synchrotron Radiation Facility (ESRF) in Grenoble (λ = 0.414 56 Å). The structure solution was carried out by direct methods with SIR2011.[13] Synchrotron powder diffraction data were collected on the same beamline (λ = 0.414 56 Å). Neutron powder diffraction data were taken at RT, at the D2B line (λ = 1.594 Å) of the Institut Laue-Langevin (ILL) in Grenoble. The structure refinement was carried out simultaneously from the single-crystal data, synchrotron powder data, and neutron powder data with the Jana2006 software.[14] The thermal evolution of the structure was characterized also by neutron diffraction at the D20 (λ = 2.41 Å) beamline from 2 K to RT and for two selected temperatures, 140 and 200 K, at the D2B (λ = 1.594 Å) line of the ILL in Grenoble.

Pyroelectric currents for the study of electric polarization were measured on a metalized sample of 0.5 mm × 8 mm^2 using a Keithley electrometer 6517B for electric current detection and a Keithley 2400 Source Meter Unit for sample poling. Electrical resistivity was measured on the same sample in a two contacts configuration. The dielectric constant was measured with an LCR meter HP4824A covering the frequency range from 20 Hz to 1 MHz applying a sinusoidal signal of 50 mV. To avoid contact effects the sample was covered by mica linings and measured according to the technique reported in ref 15. Temperature was controlled by inserting the devices under test in the SQUID magnetometer sample chamber. The study of the ferroelectric properties of Pb_2MnWO_6 was carried out at 292 K by means of AIXACCT TF-Analyzer 2000E ferroelectric tester. A thin disc, with thickness of t = 200 μm and area of A = 7.02 mm^2, was lapped and metalized with a 20 nm layer of platinum by sputtering technique approximating a parallel plate capacitor.

RESULTS AND DISCUSSION

RT Crystal Structure and Low-Temperature Trend. Laboratory PXRD diffraction data were indexed with a superstructure related to the simple perovskite cell by $\mathbf{a} = 2\mathbf{a}_p$, $\mathbf{b} = \sqrt{2}\mathbf{a}_p$, and $\mathbf{c} = 2\sqrt{2}\mathbf{a}_p$. A minor impurity phase (less than 5%) was detected and identified as lead tungstate $PbWO_4$. The RT structure was solved ab initio from synchrotron single-crystal data collected at the D09A beamline of the ESRF by the application of direct methods in the noncentrosymmetric space group $Pmc2_1$. This is in contrast with the previously published *Pnma* structure refined on the basis of powder diffraction,[9] but it must be noticed that owing to the weak intensity of the superstructure reflections and to their superimposition in powder diffraction, the correct identification of the space group is possible only through the analysis of the systematic absences in single-crystal data. According to the observed systematic absences (h0l with $l = 2n + 1$), the structure solution was attempted in the *Pmcm*, *Pmc*2, and $Pmc2_1$ space groups, the latter only giving a reasonable solution. The actual $Pmc2_1$ symmetry represents a maximal nonisomorphic subgroup with respect to the proposed *Pnma* structure. Consequently, this new setting determines the splitting of each atomic position of the double perovskite. Therefore, in the new structural model the independent atomic positions are 16 instead of 8. To comply with the symmetry constraint of $Pmc2_1$ it is also necessary to adopt a new crystallographic orientation of the lattice, obtained through the following transformation:

$$\begin{pmatrix} \mathbf{a}' \\ \mathbf{b}' \\ \mathbf{c}' \end{pmatrix} = \begin{pmatrix} 0 & 1 & 0 \\ 0 & 0 & 1 \\ 1 & 0 & 0 \end{pmatrix} \begin{pmatrix} \mathbf{a} \\ \mathbf{b} \\ \mathbf{c} \end{pmatrix}$$

wherein **a**, **b**, and **c** refer to the published model,[9] and **a**′, **b**′, and **c**′ correspond to the new setting of axes.

Since the experimental setup used for single-crystal diffraction is generally suited for high-pressure experiments, the exploration of the overall reciprocal space was precluded, and only a limited number of reflections was collected. Therefore, to achieve reliable structural information, the refinement was simultaneously carried out using single-crystal synchrotron data, powder synchrotron data, and neutron data. The atomic displacement parameters (ADPs) of the Pb atoms were refined anisotropically, whereas isotropic ADP was used for all the remaining sites; to stabilize the refinement all the ADPs for the oxygen atoms were constrained to the same value. The Rietveld plots, showing a good agreement between observed and calculated patterns, are reported in Figure 1, while the Rietveld plots of the 140 and 210 K neutron data are reported as Supporting Information. The global crystallographic information is presented in Table 1, while atomic coordinates are reported in the Supporting Information with a selection of bond lengths. On the basis of the refinement results, the B site of the perovskite structure was found to be completely ordered, with Mn and W atoms located in a NaCl-like arrangement as shown in Figure 2. The different volumes of the respective coordination octahedra, joined to the large valence gap, represents the driving force for the ordering. The bond valence sums evaluated with the CHARDIS99 software,[16] specifically designed for systems with distorted coordinations, are very close to the theoretical value for all the ions in the

dx.doi.org/10.1021/ic501328s | Inorg. Chem. 2014, 53, 10283−10290

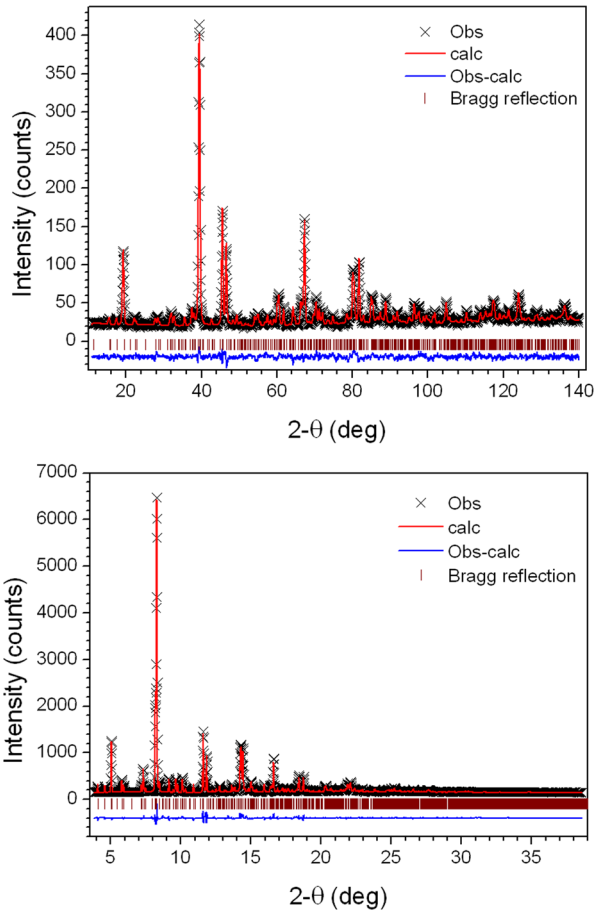

Figure 1. Rietveld plots related to the structural refinements of the Pb_2MnWO_6 perovskite at RT based on neutron (top) and synchrotron (bottom) powder diffraction data. Observed (×, black), calculated (line, red), and difference (line, blue) pattern are reported. The tickmarks show the calculated position of the Bragg reflections.

Table 1. Crystal Data and Refinement Parameters

chemical formula		Pb_2MnWO_6	
space group		$Pmc2_1$	
a (Å)		8.0370(2)	
b (Å)		5.7857(2)	
c (Å)		11.6378(4)	
V (Å^3)		541.15(3)	
Z		4	
D (g cm^{-3})		9.1923	
	single-crystal XRD	powder XRD	powder neutron diffraction
λ (Å)	0.414 556	0.414 556	1.594
GOF	1.51	0.66	1.50
R	0.0245	0.0294	0.0512
R_w	0.0245	0.0465	0.0600
overall GOF		1.14	

structure. The octahedral network shows a very limited tilting in the **bc** plane, as pointed out by the value of the W−O−Mn bond angles ranging from 170 to 180°. On the contrary, along **a**, the stereochemical effect of the lead atoms induces a large displacement of the apical oxygens forcing the W−O−Mn angles to decrease, in one case to the 164° limit.

The coordination environments of the two independent lead atoms are strongly asymmetric, as expected from the stereo-

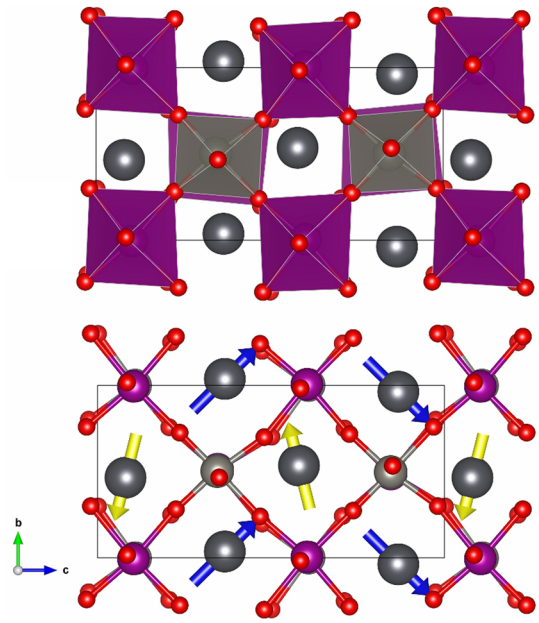

Figure 2. (top) Projection of the PMW structure onto the **bc** plane, where violet and gray polyhedra refer to Mn and W atoms, respectively, while the black spheres indicate the Pb atoms; (bottom) displacements scheme of the Pb atoms, giving rise to a net dipolar moment along **c**.

activity of the 6s^2 lone pair,[17] and differ in terms of local distortion and average bond lengths, that are 2.94(15) Å and 2.86(17) Å for Pb1 and Pb2, respectively. While Pb1 forms four almost equivalent short bonds, ranging from 2.49 to 2.60 Å, the distortion of the Pb2 coordination is more pronounced, giving rise to three shorter bonds ranging from 2.33 to 2.56 Å. Both types of environments are typically found in lead oxides, where $Pb1O_4E$ and $Pb2O_3E$ (E stands for lone pair) coordinations are usually observed.[18] The refined anisotropic ADPs for both the lead cations are consistent with the values found for the rest of the atomic species. Concerning the previously published structure,[9] uncommon high values of isotropic ADP for the Pb site were reported and, as a result, the occurrence of some local structural distortion was suggested. Indeed the larger ADP parameters were probably determined by the merging of two independent atomic positions for the atoms in the centrosymmetric *Pnma* symmetry.

Asymmetric environments are detected also in the BO_6 coordination polihedra. The magnitude of the octahedral distortions Δd, calculated according to Halasyamani,[18] result to be in the range of a weak distortion for the manganese atoms (Δd = 0.29 and 0.19 Å for Mn1 and Mn2, respectively), whereas the tungsten atoms are significantly more distorted showing Δd = 0.35 Å for W1 and Δd = 0.37 Å for W2. The distortion of the octahedral site in classical ferroelectric perovskites, constituted by high-valent d^0 cations (typically Ti^{4+}), mainly relies on second-order Jahn−Teller (SOJT) effect. This type of distortion is consistent with the W^{6+} ion valence condition; on the other side it was shown by I. B. Bersuker[19] that such SOJT effect is theoretically possible also for Mn^{2+} in d^5 high spin configuration.

The two sublattices generated by the lead atoms are evidenced in Figure 2, the arrows show the direction of the displacements organized in rows parallel to the **a** axis. Both the sublattices produce nonzero polarization components that are

dx.doi.org/10.1021/ic501328s | *Inorg. Chem.* 2014, 53, 10283−10290

coupled antiferroelectrically along the **c** axis but, being unbalanced, they give rise to a net dipolar moment. A similar situation involves the B sites and analogously to the Pb sites, the displacements of the Mn and W species are coupled in an antipolar way on the x = 0 and x = 0.5 planes, as shown in Figure S2 in the Supporting Information. However, also in this case the localized distortions are uncompensated, resulting in a not negligible dipolar moment directed along the **c** axis, accordingly to the one generated from the lead sublattices. If all the contributions are considered, the structure of the PMW perovskite can be regarded as a complex ferrielectric system, in which **c** represents the polar axis. The lack of perfect antipolar order can be definitely ascribed to the absence of the inversion center. The strongly active role of the $6s^2$ lone pair of the lead atoms[17] must be considered as the main driving force in influencing the magnitude and direction of the polar displacements.[18]

The evolution of the crystal structure with temperature was studied by PXRD data collected between 90 and 500 K and by neutron powder diffraction (NPD) data obtained at the D20 line between 2 K and RT. The measurements confirmed the occurrence of a structural transition at 450 K from a paraelectric cubic perovskite structure to the electrical ordered orthorhombic one, as reported by Blasco et al.[9] The transition is analyzed in Figure 3 in terms of thermal evolution of the

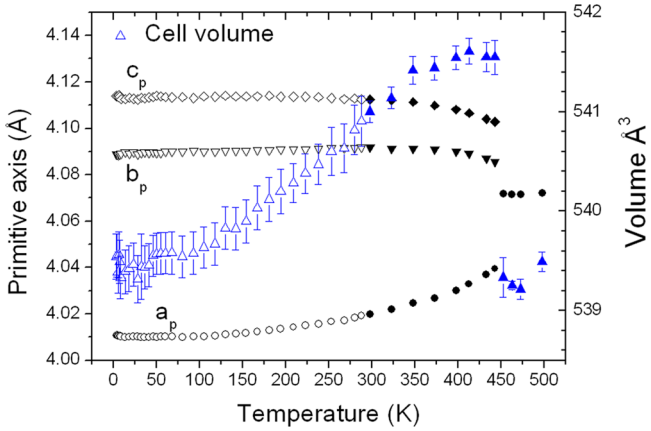

Figure 3. Lattice parameters of PMW as a function of temperature, reported in terms of fundamental perovskite cell. On the right axis is reported the trend of the unit cell volume versus temperature, from which a first-order phase transition at 450 K is evident. The empty symbols refer to neutron data, the filled ones to XRD data.

fundamental perovskite cell parameters, revealing the occurrence of an expansion in two crystallographic dimensions, resulting from the lead atoms distortions, which increase by lowering the temperature, and a compression in the third one, produced by the progressive bending of the apical B−O bonds. With regards to the temperature region above 200 K, a series of feeble structural distortions with a typical anisotropic nature are encountered on cooling. The amplitude of these lattice variations is certainly tiny, but they can be correlated to the changes of the electric properties reported in the following section.

At first, it is possible to note around 170 K a change in the slope of the **c** axis of the structure (Figure 4a), while the other two axes maintain the expected thermal evolution. As already emphasized, the **c** axis corresponds to the polar direction in the $Pmc2_1$ space group and is strictly related to the ferrielectric

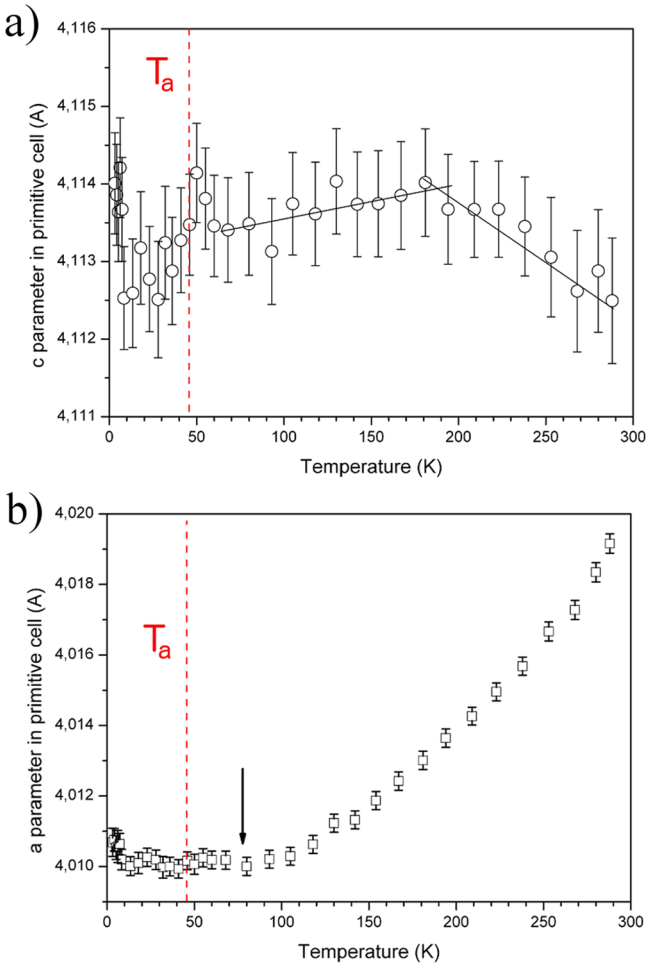

Figure 4. (a) Thermal evolution of the pseudoperovskite **c** cell parameter as a function of temperature. The change observed around 170 K is highlighted by the straight lines, which are a simple guide to the eye. (b) Thermal dependence of the perovskite **a** cell parameter. The critical point is indicated by the arrow. In both figures the magnetic anomaly at T_a, reported in ref 9, is depicted with a dashed red line.

distortion of the system. Down to the 45 K limit close to the onset of antiferromagnetic transition an abrupt change of the **c** lattice parameter takes place; in addition below 10 K in NPD pattern new reflections are observed, reasonably indicating a long-range magnetic order below this temperature. This sudden contraction alongside the polar direction, joined with the appearance of possible magnetic reflections below 10 K, could be related to some magnetostrictive effects corresponding to a possible multiferroic coupling. As far as the powder diffraction experiments revealed, the change of the thermal expansion coefficient of the polar direction around 170 K did not coincide with any further phase transition related to symmetry switching. Interestingly, as illustrated in Figure 4b, the **a** parameter shows, close to 80 K, a remarkable change of the temperature dependence of its value. This crystallographic direction corresponds to the major octahedral tilting distortion of the double Mn/W framework, and the observed freezing could be related to the reaching of the maximum limit of such deformation.

Electrical Characterization. The polarization reversal induced by applied electric field on a PMW sample, whose preparation conditions are detailed in the Experimental Section,

dx.doi.org/10.1021/ic501328s | *Inorg. Chem.* 2014, 53, 10283−10290

is illustrated in Figure 5. After a high voltage static treatment, a Positive Up Negative Down measurement (V = 2000 V, f = 5

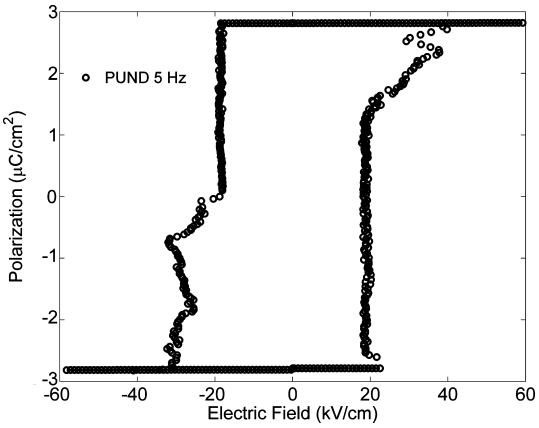

Figure 5. FE-hysteresis measurement performed with a Positive Up Negative Down (PUND) protocol for an applied voltage pulse of maximum amplitude 2000 V and frequency 5 Hz after a specific DC poling treatment to write the dipole in the structure.

Hz) allowed to individuate an hard hysteresis loop in the polarization of PMW (Figure 5) with a symmetric coercive electric field E_C = 20 kV/cm and a saturation polarization P_S = 2.85 μC/cm^2. This measurement is completely reproducible and all the spurious contributions, as for example leakage currents and resistive/dissipative contributions are completely negligible with respect to the used voltage ranges, pulse frequencies and temperature conditions. The remarkable coercivity of PMW close to the standard values obtained for lead zirconate titanate (PZT),[20] could be probably overestimated. Indeed, the observed critical field in an inhomogeneous and polycrystalline system has to be properly redefined as a sum of two terms: the real coercive electric field (i.e., the intrinsic parameter of the structural electric dipole) and a specific depinning field, which depends on the sample microstructure, due to the presence of morphological defects and grain boundary effects.

A series of distinctive elements of this loop can be considered as indicative of a ferrielectric state. The phenomenology of polarization reversal of ferrielectrics has been investigated by C. F. Pulvari by analyzing the electric behavior of mixed niobates[21] and bismuth titanates.[22] On the basis of Pulvari's observations the opening of the ferrielectric hysteresis requires higher electric fields with respect the coercive force of the system. Indeed, irrespectively of the classical ferroelectric phenomenology, in which the switching transients are characterized by a smoothed evolution to saturation, the polarization is characterized here by a sudden onset above a critical switching field. The presence of this threshold is emphasized by the fact that below a certain field the hysteresis loop does not appear, and the material shows the behavior of a linear dielectric (as shown later). This confers to the ferrielectric hysteresis the particular square shape of the loop even in presence of a polycrystalline ceramic; a similar behavior is generally observed during the polarization of ferroelectric single crystals with strong polar crystalline anisotropy (e.g., tetragonal ferroelectric perovskites such as PZT or $BaTiO_3$).

On the other hand, in classical antiferroelectric systems the polarization is outlined by the characteristic double hysteresis loop indicating that the phase transformation to ferroelectric regime is reversible; "ferri" polar ordering can be distinguished because the transformation is irreversible being the remnant polarization persistent at E = 0. The noisy region of the hysteresis related to the shoulders detected between 20 and 40 kV/cm deserves some considerations. First of all the zigzag features, well visible in the right side of the hysteresis loop, are a pure instrumental effect. The ferroelectric tester passes in a current-limited regime any time the prepolarization current rises up abruptly over the fixed maximum value of the current range; as a consequence to prevent damages, the current is instrumentally retained, and the applied voltage is automatically reduced. On the other hand, the initial metastable-antipolar state in the PMW specimen is converted when the critical switching field is achieved. This process is not complete, and a portion of the material is likely locked to the antiferro dipole condition. In earlier studies[22] carried out on ferrielectrics this stage is recognized as an intermediate dynamical situation, which is quickly suppressed by increasing the maximal limit of the applied electric field. The possible presence of antipolar domains surviving during reversal polarization process could be ascribed to microstructural defects usually expected in ceramic sintered with standard procedure.

The direct current (dc) electrical resistivity ρ was measured from T = 90 K to T = 380 K, while for lower temperatures the insulating properties of Pb_2MnWO_6 exceed the instrumental sensitivity. Measurements were carried out with applied voltages ranging from 10 to 200 V and are reported in Figure 6. In the whole explored temperature range, the measured

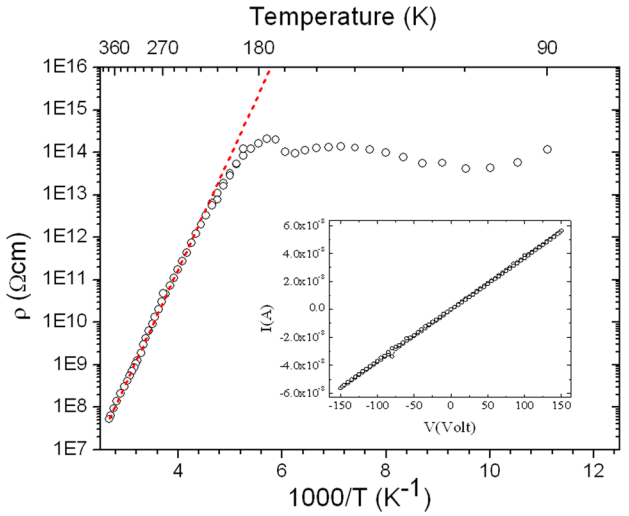

Figure 6. Electrical resistivity in the temperature range of 90−380 K for applied voltages ranging from 10 to 200 V; the dashed line corresponds to the Arrhenius best-fit with activation energy E_ρ = 0.53 eV. (inset) The $I(V)$ plot at T = 290 K, indicating that ρ does not depend on the applied voltage.

values of ρ were found to be independent of the applied voltage, as shown in the inset of Figure 6. ρ always keeps high values, strictly following a semiconducting behavior $\rho = \rho_0 \exp(E_\rho/kT)$, to T = 230 K at least, with activation energy E_ρ = 0.53 eV; a clear anomaly is observed at T = 170 K, connected with a drastic change in the temperature dependence of the resistivity.

The sample shows high values of the dielectric constant. The evolution of the relative dielectric constant versus temperature is shown in Figure 7, revealing the existence of a dielectric

dx.doi.org/10.1021/ic501328s | Inorg. Chem. 2014, 53, 10283−10290

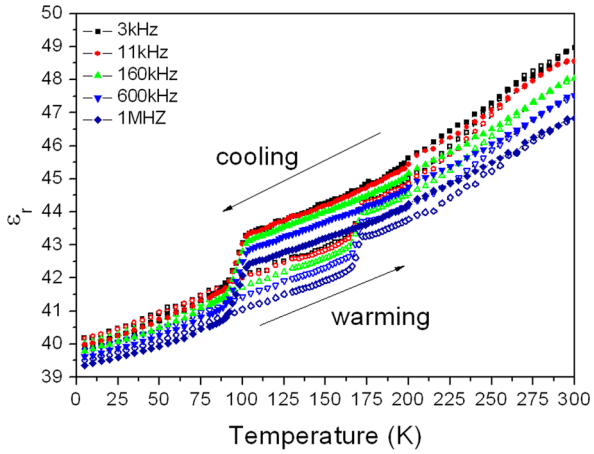

Figure 7. Dielectric constant in the temperature range of 5−300 K measured on cooling (full symbols) and on warming (empty symbols).

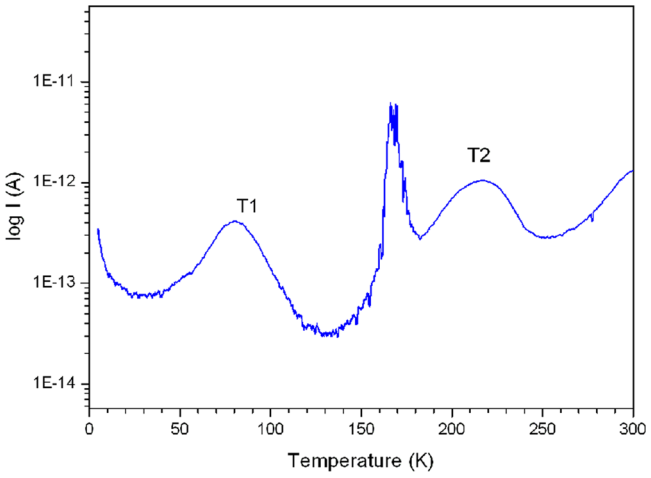

Figure 8. Depolarization curves for E_0 = 3125 V/cm and T_p = 380 K. T_1 and T_2 indicate the broad peaks cited in the text.

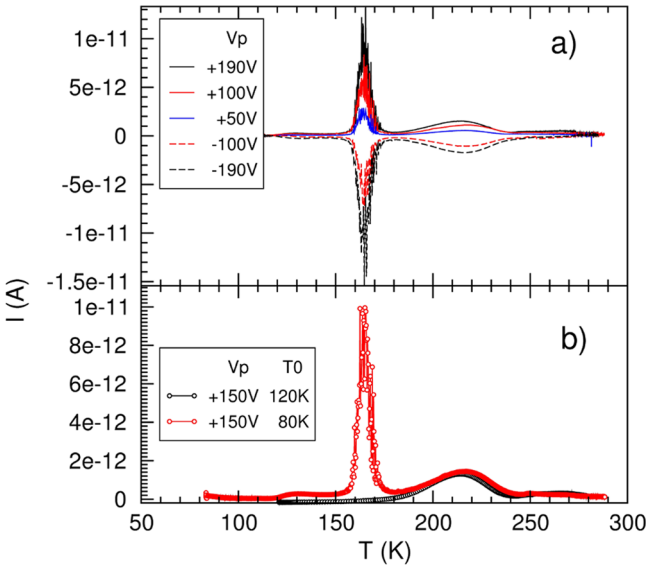

Figure 9. Depolarization curves for poling temperature T_p = 273 K and: (a) different poling voltages V_p and T_0 = 80 K; (b) poling voltage V_p = 150 V and T_0 values below and above 90 K.

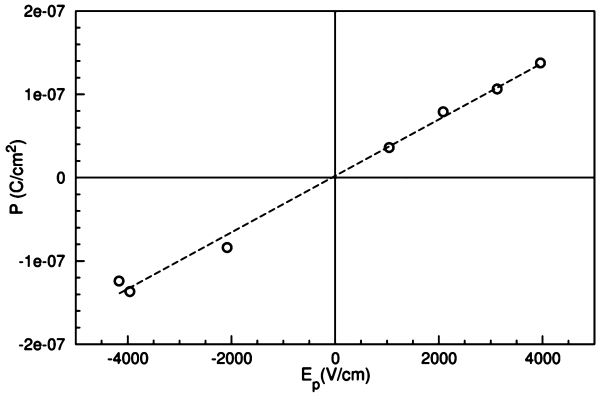

Figure 10. Static electric polarization at T_p = 273 K as a function of the poling field E_p obtained by integration of the ITC currents of Figure 9. The dashed line represents the linear best-fit of data.

transition showing a large hysteresis: a kink, observed at around 90 K in the measurements performed on cooling, is shifted to about 170 K when the measurements are recorded on warming. The transition, not affected by the frequency of the applied field, can be related with the anomaly in the resistivity measurement, which occurs at the same temperature (recall that the resistivity measurements were performed on warming). The strong thermal hysteresis observed in the dielectric measurement is consistent with a first-order transition; in spite of this, no remarkable cell volume discontinuity or space group changes were revealed by the structural characterization at this temperature. The thermal behavior of both resistivity and electrical permittivity near 170 K agrees with the hypothesized change of transport properties in the system. The conversion from a thermal activated conduction mechanism to a nearly constant value with temperature could be ascribed to a possible localization or freezing of the conduction charges. The correlation between the thermal expansion change of the polar axis of the structure and the dielectric anomaly is reasonably attributed to some electronic transition, which does not correspond to any evident crystalline transformation.

The dc electric polarization as a function of temperature was studied by means of ionic thermocurrents (ITC) measurements:[23−25] a sample is polarized at a poling temperature T_p by the application of an electric field E_p, and it is cooled to a temperature T_0 while keeping the electric field on. Then the electric field is switched off, and the sample is slowly heated at a linear heating rate to T_p or higher. During the heating process, a pyroelectric current is released by the sample: this is called ITC, and from its integration it is possible to obtain the electric polarization of the sample originated by the action of E_p. Figure 8 shows the ITC released by a sample polarized at T_p = 380 K with E_p = 3125 V/cm, which represents the maximal electric field provided by the available equipment. It is important to stress that although in these experimental conditions the threshold field to open the ferrielectric hysteresis loop (as shown in Figure 10) is not reached, the information so far collected from this type of measurement can be meaningful to gain additional insights into the observed low-temperature features. The ITC curve shows two broad and weak peaks at T_1 = 80 K and T_2 = 217 K and a narrow change at 165 K. Several ITC measurements, a selection of them shown in Figure 9, have been carried out in the range from 80 to 300 K for different values of the poling field E_p. The three anomalies are reproduced in all the different runs with unchanged character-

dx.doi.org/10.1021/ic501328s | Inorg. Chem. 2014, 53, 10283−10290

istic temperatures. The sharp peak at 165 K is clearly associated with the transformation observed in both the resistivity and the dielectric constant. Repeated ITC measurements show that this intense variation appears always at the same temperature (Figure 9a), but only if the cooling of sample exceeds 90 K (Figure 9b); this fact is consistent with the wide hysteresis observed in the dielectric constant temperature dependence. The ITC curves of Figure 9a show that the sign of the electric polarization developed around RT can be switched by the inversion of the poling voltage. On the contrary, inversion of the poling voltage at T_0 = 80 K (not shown in Figure 9) did not lead to the polarization switching because of dipole freezing at low temperature. Noteworthy, T_1 coincides with the change of the thermal expansion coefficient of the **a** lattice parameter of the orthorhombic double perovskite.

The nature of the T_1 and T_2 pyrocurrent bands is far from being understood. In conventional ferroelectric materials pyrocurrent analysis involves the observation of a clear intense peak corresponding to phase transformation to the paraelectric state at the Curie temperature T_C. For instance the 165 K anomaly assumes the expected distinctive features of a first-order transition, as pointed out by the comprehensive electric characterization. The remaining two temperatures are difficult to interpret since no additional property changes involving magnetic, structural, and electric aspects were detected. The reported ITC characterization is limited in the maximum applied voltage due to the constraints of the actual equipment; nevertheless, by means of integration of currents, one can obtain the static electric polarization of the material at T_p as a function of the applied poling field, as reported in Figure 10 for T_p = 273 K. The linear behavior and null remanence are consistent with the ferrielectric nature of Pb_2MnWO_6, though the threshold field could not be reached by means of the available voltage.

CONCLUSION

The RT stable ferrielectric state for the PMW double perovskite, featured by the presence of noncentrosymmetric $Pmc2_1$ symmetry, has been ascertained by an exhaustive structural analysis. The combination of uncompensated lattice distortions of the noncentrosymmetric crystal structure with the ferroelectric polarization reversibility indicates that the PMW compound is characterized by ferrielectricity in a wide temperature range. In addition ferrielectricity was confirmed also by the analysis of the hysteresis loop of electric polarization. In the frame of the electrical behavior of antiferroeletrics, the PMW perovskite has distinctive properties indicating the occurrence of a ferrielectric response to the application of an electric field. In agreement with the phenomenology of ferrielectrics established by the work of C. F. Pulvari[21,22] the system shows high coercive field with an irreversible remanent polarization. In principle this would imply that the structural phase showing unbalanced antipolar lattice is converted, through an electric field driven process, in a crystalline form with a clear ferroelectric ordering. The possible coexistence of this electric ordering with magnetism could open up new perspectives in the field of multiferroics. This characteristic, together with the clear magnetostrictive effect involving the polar axis at the antiferromagnetic transition temperature, indicates that Pb_2MnWO_6 is the natural candidate for the study of this multifunctional synergy. The low-temperature behavior of PMW has been widely studied by electric and structural experiments, and a series of novel critical phenomena has been explained for the first time. The most important result is represented by the anomaly observed in the temperature dependence of the dielectric constant, which assumes a clear first-order character whose occurrence affects both the resistivity and pyrocurrent outputs. Despite this remarkable anomaly observed in the electric properties at 170 K, the crystal structure of PMW is not involved in a clear transformation; the inversion of the expansion thermal coefficient of the **c** polar axis is the sole anomaly observed.

ASSOCIATED CONTENT

Supporting Information

Crystallographic information file (CIF), tables with atomic coordinates, selected bond lengths and angles, Rietveld plots of additional data. This material is available free of charge via the Internet at http://pubs.acs.org.

AUTHOR INFORMATION

Corresponding Author

*fabio.orlandi@nemo.unipr.it.

Author Contributions

All authors have given approval to the final version of the manuscript.

Notes

The authors declare no competing financial interest.

ACKNOWLEDGMENTS

The authors F.O., D.D., C.P., and M.S. thank Fondazione Cariparma for financial support. The authors are grateful to the ILL institute for making at their disposal the neutron diffraction facilities available at the D20 and D2B beamlines. The authors acknowledge Dr. C. Ritter for the realization of the powder neutron diffraction experiments and for successive fruitful discussions. The authors are grateful to the ERSF institute for making at their disposal synchrotron facilities available at the ID09A beamline.

REFERENCES

(1) Hill, N. A. *J. Phys. Chem. B* **2000**, *104*, 6694−6709.
(2) Kobayashi, K. I.; Kimura, T.; Sawada, H.; Terakura, K.; Tokura, Y. *Nature* **1998**, *395*, 677−680.
(3) Arulraj, A.; Rameshaa, K.; Gopalakrishnana, J.; Rao, C. N. R. *J. Solid State Chem.* **2000**, *155*, 233−237.
(4) Kato, H.; Okuda, T.; Okimoto, Y.; Tomioka, Y.; Takenoya, Y.; Ohkubo, A.; Kawasaki, M.; Tokura, Y. *Appl. Phys. Lett.* **2002**, *81*, 328−330.
(5) Yáñez-Vilar, S.; Mun, V. S.; Zapf, E. D.; Ueland, B. G.; Gardner, J. S.; Thompson, J. D.; Singleton, J.; Sánchez-Andújar, M.; Mira, J.; Biskup, N.; Señarís-Rodríguez, M. A.; Batista, C. D. *Phys. Rev. B* **2011**, *84*, 134427.
(6) Baldinozzi, G.; Calvarin, A.; Sciau, Ph.; Grebille, D.; Suard, E. *Acta Crystallogr.* **2000**, *B56*, 570−576.
(7) Larrégola, S. A.; Alonso, J. A.; Sheptyakov, D.; Alguerò, M.; Muñoz, A.; Pomjakushin, V.; Pedregosa, J. C. *Inorg. Chem.* **2011**, *50*, 5545−5557.
(8) Ivanov, S. A.; Nordblad, P.; Mathieu, R.; Tellgren, R.; Ritter, C. *Dalton Trans.* **2010**, *39*, 11136−11148.
(9) Blasco, J.; Merino, R. I.; García, J.; Sánchez, M. C. *J. Phys.: Condens. Matter* **2006**, *18*, 2261−2271.
(10) Catalan, G.; Scott, J. F. *Adv. Mater.* **2009**, *21*, 2463−2485.
(11) Ivanov, S. A.; Eriksson, S. G.; Tellgren, R. H.; Rundlo, R. *Mater. Res. Bull.* **2004**, *39*, 2317−2328.
(12) Subías, G.; Blasco, J.; García, J.; Herrero-Martín, J.; Sánchez, M. C. *Phys. Condens. Matter* **2009**, *21*, 075903.

(13) Burla, M. C.; Caliandro, R.; Camalli, M.; Carrozzini, B.; Cascarano, G. L.; Giacovazzo, C.; Mallamo, M.; Mazzone, A.; Polidori, G.; Spagna, R. *J. Appl. Crystallogr.* **2012**, *45*, 357−361.
(14) Petricek, V.; Dusek, M.; Palatinus, L. *Z. Kristallogr.* **2014**, *229*, 345−352.
(15) Cabassi, R.; Bolzoni, F.; Gauzzi, A.; Gilioli, E.; Prodi, A.; Licci, F. *Phys. Rev. B* **2006**, *74*, 045212.
(16) Nespolo, M.; Ferraris, G.; Ohashi, H. *Acta Crystallogr.* **1999**, *B55*, 902−916.
(17) Walsh, A.; Payne, D. J.; Egdellb, R. G.; Watsonc, G. W. *Chem. Soc. Rev.* **2011**, *40*, 4455−4463.
(18) Halasyamani, P. S. *Chem. Mater.* **2004**, *16*, 3586−3592.
(19) Bersuker, I. B. *Phys. Rev. Lett.* **2012**, *108*, 137202.
(20) Shmidt, N. A. *Ferroelectrics* **1981**, *31*, 105−111.
(21) Pulvari, C. F. *Phys. Rev.* **1960**, *120*, 1670.
(22) Pulvari, C. F.; de la Paz, A. S. *J. Appl. Phys.* **1966**, *37*, 1754−1763.
(23) Muller, P. *Phys. Status Solidi A* **1981**, *67*, 11−60.
(24) Bucci, C.; Fieschi, R.; Guidi, G. *Phys. Rev.* **1966**, *148*, 816−823.
(25) Riva, S. C.; Bucci, C. A. *J. Phys. Chem. Solids* **1965**, *26*, 363−371.